Metabolic Engineering Communications 5 (2017) 9–18

Contents lists available at ScienceDirect

Metabolic Engineering Communications

journal homepage: www.elsevier.com/locate/mec

Comparison of orthologous cyanobacterial aldehyde deformylating oxygenases in the production of volatile C3-C7 alkanes in engineered *E. coli*

Pekka Patrikainen, Veronica Carbonell, Kati Thiel, Eva-Mari Aro, Pauli Kallio*

Molecular Plant Biology, Department of Biochemistry, University of Turku (Turun Yliopisto), 20014 TURUN YLIOPISTO, Finland

ARTICLE INFO

Chemical compounds:
Propane (PubChem CID: 6634)
Pentane (PubChem CID: 8003)
Heptane (PubChem CID: 8900)
Butanoic acid (PubChem CID: 264)
Hexanoic acid (PubChem CID: 8892)
Octanoic acid (PubChem CID: 379)
Butanol (PubChem CID: 263)
Hexanol (PubChem CID: 8103)
Octanol (PubChem CID: 957)

Keywords:
Cyanobacterial aldehyde deformylating oxygenase
ADO
Volatile alkane
Short-chain hydrocarbon
Pathway engineering
Escherichia coli

ABSTRACT

Aldehyde deformylating oxygenase (ADO) is a unique enzyme found exclusively in photosynthetic cyanobacteria, which natively converts acyl aldehyde precursors into hydrocarbon products embedded in cellular lipid bilayers. This capacity has opened doors for potential biotechnological applications aiming at biological production of diesel-range alkanes and alkenes, which are compatible with the nonrenewable petroleum-derived end-products in current use. The development of production platforms, however, has been limited by the relative inefficiency of ADO enzyme, promoting research towards finding new strategies and information to be used for rational design of enhanced pathways for hydrocarbon over-expression. In this work we present an optimized approach to study different ADO orthologs derived from different cyanobacterial species in an *in vivo* set-up in *Escherichia coli*. The system enabled comparison of alternative ADOs for the production efficiency of short-chain volatile C3-C7 alkanes, propane, pentane and heptane, and provided insight on the differences in substrate preference, catalytic efficiency and limitations associated with the enzymes. The work concentrated on five ADO orthologs which represent the most extensively studied cyanobacterial species in the field, and revealed distinct differences between the enzymes. In most cases the ADO from *Nostoc punctiforme* PCC 73102 performed the best in respect to yields and initial rates for the production of the volatile hydrocarbons. At the other extreme, the system harboring the ADO form *Synechococcus* sp. RS9917 produced very low amounts of the short-chain alkanes, primarily due to poor accumulation of the enzyme in *E. coli*. The ADOs from *Synechocystis* sp. PCC 6803 and *Prochlorococcus marinus* MIT9313, and the corresponding variant A134F displayed less divergence, although variation between chain-length preferences could be observed. The results confirmed the general trend of ADOs having decreasing catalytic efficiency towards precursors of decreasing chain-length, while expanding the knowledge on the species-specific traits, which may aid future pathway design and structure-based engineering of ADO for more efficient hydrocarbon production systems.

1. Introduction

As a unique trait in the bacterial kingdom, all photosynthetic cyanobacteria characterized to date harbor the capacity to produce medium chain-length hydrocarbons in their metabolism (Coates et al., 2014). Although the biological role of the hydrocarbon products is not entirely understood, the biosynthetic pathways and the key enzymes associated with the different catalytic steps have been elucidated. The most common cyanobacterial pathway is based on the enzyme *aldehyde deformylating oxygenase* (ADO) (Coates et al., 2014), which catalyzes the conversion of fatty aldehyde substrates, generated by *fatty acyl ACP reductase* (Aar), into C_{n-1} hydrocarbons and formate [see review (Marsh and Waugh, 2013)]. Since the discovery of the biosynthetic route (Schirmer et al., 2010), there has been significant scientific interest towards ADO, due to the prospects in developing microbial over-production platforms for renewable replacements of petroleum-derived products. The endogenous pathways produce predominantly C15-C17 alkanes and alkenes, and the reported total levels are about 0,1% of dry biomass (Coates et al., 2014; Tan et al., 2011). While various strategies have been implemented to engineer the native pathways in cyanobacteria for higher yields, many heterologous pathway variants have been assembled in heterotrophic host *Escherichia coli* (*E. coli*) to produce alkanes of different lengths, from C9-C17 products (Schirmer et al., 2010; Harger et al., 2013; Akhtar et al., 2013; Howard et al., 2013; Choi and Lee, 2013) towards volatile compounds heptane (C7) (Akhtar et al., 2013; Kallio et al., 2014) and propane (C3) (Kallio et al., 2014; Menon et al., 2015; Zhang et al., 2016). Although the reported yields have remained marginal as compared to any industrially relevant process, the studies have provided detailed molecular-level insight into the essential limiting factors of the hydrocarbon pathways; stringent native regulatory systems, competing endo-

* Corresponding author.
E-mail addresses: ptpatr@utu.fi (P. Patrikainen), vecago@utu.fi (V. Carbonell), kshann@utu.fi (K. Thiel), evaaro@utu.fi (E.-M. Aro), pataka@utu.fi (P. Kallio).

http://dx.doi.org/10.1016/j.meteno.2017.05.001
Received 20 December 2016; Received in revised form 11 April 2017; Accepted 1 May 2017
Available online 08 May 2017
2214-0301/ © 2017 The Authors. Published by Elsevier B.V. on behalf of International Metabolic Engineering Society. This is an open access article under the CC BY-NC-ND license (http://creativecommons.org/licenses/BY-NC-ND/4.0/).

genous pathways, and unoptimal catalytic properties of the associated enzymes which compromise the output.

ADO has been extensively characterized in respect to catalytic mechanism, kinetic properties and structure. ADO is a soluble ferritin-like di-iron oxygenase which catalyzes the C1-C2 bond cleavage of aldehyde substrates into a corresponding C_{n-1} alk(a/e)ne and formate *via* a multi-step free-radical mechanism (Paul et al., 2013; Rajakovich et al., 2015; Jia et al., 2015). ADO uses molecular oxygen as a cosubstrate, and the reaction results in the incorporation of one oxygen atom into formate while the other atom is reduced to H_2O (Warui et al., 2011). The reaction is dependent on an external reducing system to provide altogether four electrons for the (i) activation of the di-iron center for oxygen binding, (ii) hemiacetal radical formation, and (iii) generation of the product complex (Paul et al., 2013; Rajakovich et al., 2015). Characteristically, ADO has relatively broad substrate specificity towards different aldehydes, with the highest activity towards the native linear C16 and C18 precursors (Khara et al., 2013; Bao et al., 2016; Zhang et al., 2016). This feature is accompanied by a low apparent catalytic turnover rate with reported k_{cat} values below 0.02 s^{-1} in different contexts *in vitro* and *in vivo* (Khara et al., 2013; Andre et al., 2013; Bao et al., 2016). Kinetic characterization has also revealed that the affinity towards the aldehyde substrates is poor, especially for the shorter precursors, with K_M values in the millimolar range (Bao et al., 2016). As the intracellular concentration of potentially toxic aldehyde intermediates must be maintained relatively low, ADO is expected to function below saturating substrate concentrations, and consequently, the apparent turnover rates are very low. This makes the ADO-catalyzed step one of the primary limiting factors forestalling the development of efficient hydrocarbon pathways, which cannot be effectively compensated by simple enzyme over-expression strategies alone. It has been postulated that the performance of ADO is associated with the labile nature of the di-iron center involved in the catalysis (Jia et al., 2015), suggesting that additional information on mechanistic structure-function studies could enable strategies of further enhancing the ADO activity.

Different approaches have been taken to overcome the limitations and to enhance the performance of the hydrocarbon pathways for better productivity and yield. Enzyme over-expression has been used to compensate for poor catalytic activity of ADO and to improve precursor availability in the native cyanobacterial hosts (Hu et al., 2013; Wang et al., 2013; Kaiser et al., 2013), while removal of endogenous pathways competing for the pathway intermediates has been shown to improve the flux towards the target hydrocarbon products (Kallio et al., 2014; Sheppard et al., 2016; Song et al., 2016). Optimization of the redox system to ensure sufficient flow of electrons to ADO has been accomplished by overexpressing ferredoxin (Fdx) and NADPH/ ferredoxin/flavodoxin-oxidoreductase (Fpr) (Kallio et al., 2014) or by engineering an ADO-Fdx fusion protein for higher activity (Wang et al., 2014). In addition, structure-based enzyme engineering of ADO has been utilized to alter the substrate preference towards specific aldehyde precursors (Khara et al., 2013; Hayashi et al., 2015; Zhang et al., 2016; Bao et al., 2016; Sheppard et al., 2016), thus enhancing the relative yield of the corresponding hydrocarbon products. Despite the advances, the efficiency of the enzymatic conversion remains to be insufficient to enable commercial applications, and alternative strategies are needed to identify and alleviate the key metabolic bottlenecks.

In order to gain further insight into the existing natural diversity of ADOs, the aim of the study was to characterize orthologous enzymes from different sources and to evaluate enzyme-specific differences in catalytic performance in heterologous biosynthetic context *in vivo*. The approach was to assemble a set of parallel biosynthetic hydrocarbon pathways in *E. coli* with a selection of over-expressed ADOs, a carboxylic acid reductase (CAR), and a reduction system based on cyanobacterial ferredoxin PetF (Fdx) (Fig. 1). To avoid primary complications with substrate availability, the strategy was to use externally supplemented fatty acid precursors of different lengths, with the focus specifically on volatile C3-C7 end-products. Such *in vivo* comparison has not been conducted earlier, and is expected to provide information for further structure-based evaluation, and identification of enzyme-specific features associated with substrate specificity or catalytic activity.

2. Materials and methods

2.1. Reagents and enzymes

Standard molecular biology procedures and commercial kits (Qiagen) were used for DNA plasmid isolation and manipulation. All the used enzymes were purchased from New England BioLabs or from Thermo-Scientific Fermentas. All chemicals used in this study were purchased from Sigma-Aldrich if not mentioned otherwise.

2.2. Cell strains and growth conditions

Escherichia coli strain DH5α was used as the host in expression plasmid assembly. The *E. coli* strain BL21(DE3)Δ*yjgB* Δ*yqhD* (Kallio et al., 2014) which lacks the two endogenous aldehyde reductases *yqhD* and *ahr* competing with ADO for the aldehyde precursors, was used for the quantitative production experiments. The *E. coli* cells were routinely cultivated in Luria-Bertani (LB) medium at 37 °C in a shaker at 150–200 rpm or on the solid LB plates containing 1.5% (w/v) agar. The details of the production cultures are described below.

2.3. Expression plasmid construction for heterologous production of alkanes in E. coli

All plasmids, genes and organisms used in this study are listed in Table 1.

The genes coding for ADO from *Synechocystis* sp. PCC 6803 (GenBank ID: WP_010873444), *Nostoc punctiforme* PCC 73102 (GenBank ID: WP_012408400) and *Synechococcus* sp. RS9917 (GenBank ID: ZP_01080370) were ordered as synthetic fragments codon-optimized for *E. coli* (GenScript) in pUC57 with the His-tag coding regions as shown in Table 2, flanked by the restriction sites *Nco*I and *Avr*II. The *Nco*I-*Avr*II fragments were subcloned from the pUC57 into the commercial plasmid pCDF-Duet (Novagen) to obtain the corresponding final constructs pCDF-ado (*N. punctiforme*), pCDF-ado (*Synechococcus*) and pCDF-ado (*Synechocystis*) (Table 1). The codon-optimized genes encoding for the ADO from *Prochlorococcus marinus* (GenBank ID: WP_011130600) and the corresponding variant A134F were obtained from pET-28b(+) -based expression plasmid (Das et al., 2011) and a modified derivative (Khara et al., 2013), respectively. The genes were subcloned (*Nco*I-*Bam*HI) from pET-28b(+) into the pCDF-Duet to obtain the final constructs pCDF-ado (*P. marinus*) and pCDF-ado$_{A134F}$ (*P. marinus*) (Table 1) with the His-tag coding regions as shown in Table 2.

In addition to the alternative pCDF-ado constructs, the engineered system constituted of two other plasmids which allowed the simultaneous expression of the remaining four enzymes required in the alkane pathway (see Fig. 1). Ferredoxin (from *Synechocystis*), phosphopantetheinyl transferase (from *Bacillus subtilis*) and carboxylic acid reductase (from *Mycobacterium marinum*) were expressed from pET-FPC (Table 1). The construct pET-FPC was prepared by subcloning the *fdx* fragment (*Nco*I-*Hin*dIII) from pCDF-PPC (Kallio et al., 2014) to replace *tesA* in pET-TPC (Akhtar et al., 2013). NADPH: ferredoxin/flavodoxin-oxidoreductase (from *E. coli* K-12) was expressed from pACYC-fpr (Table 1). The construct pACYC-fpr was prepared by removing *petF* from existing pACYC-petF-fpr (Kallio et al., 2014) by preparative digestion (*Hin*dIII-*Nco*I), followed by blunting with Mung bean nuclease and re-ligation.

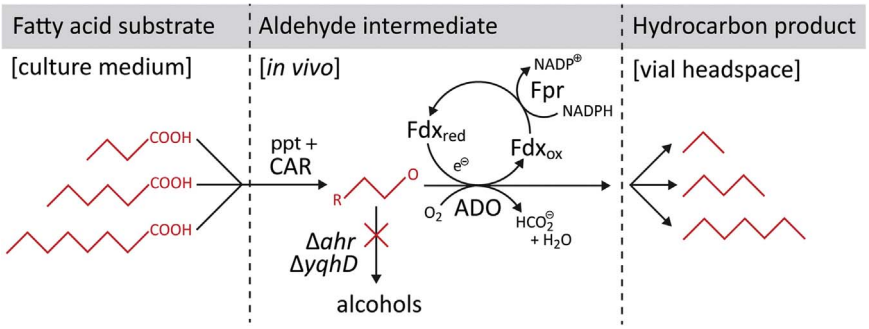

Fig. 1. Schematic representation of the hydrocarbon production system assembled in *E.coli*. The C4, C6 and C8 fatty acid substrates supplemented one at a time into the culture medium (left pane) are taken up by the *E. coli* cells. Inside the cells the fatty acid precursors are converted into aldehydes by heterologously expressed carboxylic acid reductase (CAR), assisted by the maturase phosphopantetheinyl transferase (ppt), and further into C_{n-1} alkanes by the aldehyde deformylating oxygenase (ADO) (middle pane). The reduction of ADO is accomplished by the combined action of ferredoxin (Fdx) and NADPH: Ferredoxin/Flavodoxin-oxidoreductase (Fpr). The endogenous aldehyde reductases *ahr* and *yqhD*, which compete with ADO for the aldehyde intermediates, have been deleted from the production strain. The resulting C3, C5 and C7 hydrocarbon products diffuse out of the cells and into the headspace of the closed reaction vials (right pane), and are quantitated from the gas phase by GC-MS against commercial standards for propane, pentane and heptane, respectively.

2.4. Evaluation of performance of the different ADO orthologs in hydrocarbon biosynthesis in vivo

Cultivation of the production strains (Table 1) was based on a method optimized earlier (Kallio et al., 2014); 5 ml overnight pre-cultures were grown in Luria-Bertani (LB) medium at +37 °C, and used to inoculate 50 ml main-cultures in Terrific Broth (TB) medium at +37 °C. The cultures were carried out in the presence of 100 μg ml^{-1} ampicillin, 50 μg ml^{-1} spectinomycin (omitted from the main culture), 20 μg ml^{-1} streptomycin and 34 μg ml^{-1} chloramphenicol to maintain selection pressure for the three expression plasmids. Enzyme over-expression was induced by the addition of β-D−1-thiogalactopyranoside (IPTG; 1 mM) at OD_{600} 0.5, and cultivation was continued at +30 °C for 4 h. The cells were then pelleted (+4 °C, ~4700 g, 10 min) and re-suspended into 20 ml of 100 mM potassium phosphate buffer (pH 7.5) containing 25 g l^{-1} glucose and 1 mM IPTG. In order to provide substrates for hydrocarbon biosynthesis, the cultures were supplemented with 5 mM butanoic acid, 5 mM hexanoic acid or 5 mM octanoic acid for the production of propane, pentane or heptane, respectively. Samples of 0.5 ml from the re-suspended cells were transferred to 2 ml gas-tight GC vials, sealed and incubated in a rotating shaker at RT for 30 min, 1.5 h, 2.5 h, 4 h and 10 h. Three parallel samples were prepared for GC-MS analysis in each timepoint and timepoints 30 min, 1.5 h, 2.5 h and 4 h were analyzed in a separate experiment from the 10 h timepoint.

2.5. GC-MS analysis of the volatile alkanes

Alkanes were analyzed from the headspace of sealed reaction vials using a 7890 A GC (Agilent) and 5975 C inert MS (Agilent) system with a Supelco Equity-1 (300 °C, 30 m x 0.32 mm x 1 μm) (propane) or Agilent HP-INNOWax (260 °C, 30 m x 0.32 mm x 0.5 μm) (heptane and pentane) column as described previously (Kallio et al., 2014).

Propane, pentane and heptane eluted at ~1.2 min, ~1.2 min and ~1.4 min, respectively, and were quantified by relating the GC-MS peak areas (m/z=43, 43 and 57, respectively) to corresponding commercial standards. The propane standard was a 1% mixture (v/v) in N_2 gas (AGA, Finland). The concentration series for pentane (Figure SI2) and heptane (Figure SI3) were obtained by diluting liquid standards in acetone and filled to 0.5 ml with TB medium in sealed 2 ml reaction vials, followed by 30 min incubation at +30 °C before headspace GC-MS analysis. Four replicates were analyzed in all cases, and the values were used for calculating the averages and standard deviations.

2.6. Evaluation of alcohol production of the ADO-expressing strains

For quantitating butanol, hexanol and octanol produced by the parallel strains, the reaction cultures were prepared as described in Section 2.4 for alkanes. At 10 h reaction timepoint the cell suspensions were mixed with acetone (1:1 for C4 and 1:19 for C6/C8) and the

Table 1
The host organism, plasmids and genes used in this study.

Host			**Reference**
E. coli BL21 (DE3)ΔyqhDΔahr			(Kallio et al., 2014)
Plasmid	**Genes to be expressed**		**Reference**
pET-FPC	*fdx, ppt, car*		This study
pACYC-fpr	*fpr*		This study
pCDF-ado (*N. punctiforme*)	*ado*: *Nostoc punctiforme* PCC 73102		This study
pCDF-ado (*P. marinus*)	*ado*: *Prochlorococcus marinus* MIT9313		This study
pCDF-ado$_{A134F}$ (*P. marinus*)	*ado*: *Prochlorococcus marinus* MIT9313		This study
pCDF-ado (*Synechococcus*)	*ado*: *Synechococcus* sp. RS9917		This study
pCDF-ado (*Synechocystis*)	*ado*: *Synechocystis* sp. PCC 6803		This study
Genes	**Function**	**Origin**	**GenBank ID**
fdx	Ferredoxin I	*Synechocystis* sp. PCC 6803	AAB72025.1
ppt	Phosphopantetheinyl transferase	*Bacillus subtilis*	X65610.1
car	Carboxylic acid reductase	*Mycobacterium marinum*	ACC40567.1
fpr	NADPH: ferredoxin/flavodoxin-oxidoreductase	*Escherichia coli* K−12	AAB03056.1
yqhD	Aldehyde reductase	*Escherichia coli* BL21(DE3)	ACT44688.1
ahr	Aldehyde reductase	*Escherichia coli* BL21(DE3)	AAA97166.1

Table 2
The sequence around the 5′ region of the *ado* expression constructs (Table 1) showing the RBS (yellow highlight), start codon (red), His-tag coding region (underline) and the beginning of the *ado* sequence (grey).

Plasmid	Sequence
pCDF-ado (*N. punctiforme*)	TTTAACTTTAATAAGGAGATATACCATGGCACACCACCACCACCACCACCAACAA…
pCDF-ado (*Synechococcus*)	TTTAACTTTAATAAGGAGATATACCATGGCACATCATCATCACCACCACACTCAG…
pCDF-ado (*P. marinus*)	TTTAACTTTAATAAGGAGATATACCATGGCACATCATCATCACCACCATATGCCG…
pCDF-ado (*Synechocystis*)	TTTAACTTTAATAAGGAGATATACCATGGCACATCATCATCACCACCACCCCGAG…

soluble phase was subjected to GC-MS analysis. The GC-MS set-up was the same as for heptane and pentane, operated in the split-less mode (1.4 ml min^{-1} He flow, injector at 250 °C, 2 min at 40 °C then to 250 °C with 20 °C min^{-1}, hold at 250 °C for 2 min). The amount of butanol (t_R ~5.4 min), hexanol (t_R ~7.0 min) and octanol (t_R ~8.5 min) was calculated based on the GC-MS peak areas ($m/z = 56$) of the corresponding commercial standards. The standard concentration series (0–150 mg/L were prepared in water from 1 g/L stock solutions (1:10 acetone: water)), incubated at RT for 2 h under rotation, and analyzed to obtain the standard curves for butanol (Figure SI4), hexanol (Figure SI5) and octanol (Figure SI6).

2.7. Analysis of the ADO expression levels in different strains

For evaluating ADO levels in the cells, the expression strains were cultivated as described for the alkane production experiments until the re-suspension of the cells into 100 mM potassium phosphate buffer (pH 7.5), supplemented with 25 g l^{-1} glucose, 1 mM IPTG and 50 μg ml^{-1} kanamycin. The cell suspensions were then adjusted to the same cell density ($OD_{600\ nm}$), and 6 ml aliquots were incubated in 15 ml screw capped tubes at RT in a rotational mixer for 0 h, 4 h or 10 h. After incubation, the cells were pelleted (+4 °C, ~4700 g, 10 min) and stored at –20 °C until analysis.

The His-tagged ADO enzymes were extracted by Ni^{2+} affinity chromatography using Ni-NTA Spin Columns (Qiagen) according to manufacturer's protocol for protein purification under native conditions from *E. coli* lysates. The bound ADO enzymes were eluted from column with 3 × 200 μl elution buffer (50 mM NaH_2PO_4; 300 mM NaCl; 500 mM imidazole; pH 8.0) and glycerol was added to final concentration of 40% before storage at –20 °C. The ADO expression levels and stability were evaluated using the Bradford dye-binding method (Bradford, 1976) and commercial sodium dodecyl sulfate polyacrylamide gel electrophoresis (SDS-PAGE) (12% Mini-PROTEAN® TGX™, Bio-Rad).

The protein concentrations estimated by Bradford were normalized to the sample $OD_{600\ nm}$ values in order to compare samples containing different amount of cells. The SDS-PAGE analysis was used to confirm the purity of the protein samples and to verify the ADO expression levels calculated based on the Bradford analysis.

2.8. Computational methods used for amino acid sequence alignment, enzyme structure analysis and mRNA secondary structure prediction

The amino acid sequences of the ADO orthologues were compared by using the Basic Local Alignment Search Tool BLAST web server (http://blast.ncbi.nlm.nih.gov/Blast.cgi) (Altschul et al., 1990). Sequence alignment was prepared using Clustal Omega multiple sequence alignment tool from the EMBL-EBI web pages (http://www.ebi.ac.uk/Tools/msa/clustalo). The secondary elements were included into sequence alignment using ESPript web server (http://espript.ibcp.fr/ESPript/ESPript) (Robert and Gouet, 2014). The structural analysis of the *S. elongates* PCC 7942 ADO crystal structure with bound C16 fatty alcohol (PDB code 4RC5) was done with PyMOL 1.7.4.5 (Schrödinger, LCC). The secondary structures of ADO mRNA transcripts (either the first 170 bp from the transcription start site of the T7 promoter or the whole transcript from the T7 promoter to the T7 terminator) were predicted with the Predict a Secondary Structure Web Server (http://rna.urmc.rochester.edu/RNAstructureWeb) using the default settings of the server (Reuter and Mathews, 2010).

3. Results

3.1. Sequence comparison of ADO orthologues

Native orthologous ADO enzymes from *Nostoc punctiforme* PCC 73102 (*N. punctiforme*), *Synechocystis* sp. PCC 6803 (*Synechocystis*), *Synechococcus* sp. RS9917 (*Synechococcus*) and *Prochlorococcus marinus* MIT9313 (*P. marinus*) and the *P. marinus* variant A134F were selected as the targets for the *in vivo* comparison. Alignment of the native amino acid sequences revealed 48% −68% sequence identities between the ADOs, while the overall structure, active site topology, and catalytic mechanism were expected to be rather conserved between the enzymes. The highest similarity was observed between the ADOs from *N. punctiforme* and *Synechocystis* (amino acid sequence identity 75%), whereas the ADO from *Synechococcus* appeared to be more diverged (amino acid sequence identity 40–41%), and was included in the comparison specifically as an outlier. The 17 amino acid residues within 4 Å distance from the bound C16 fatty alcohol ligand in the crystal structure of *S. elongatus* PCC 7942 (Jia et al., 2015), were all conserved between the enzymes from *P. marinus*, *N. punctiforme* and *Synechocystis* (Fig. 2). The ADO from *Synechococcus*, in comparison, carried two conservative substitutions (I17V and I104V; numbering according to the amino acids visible in the A chain of *S. elongatus* PCC 7942 crystal structure with PDB code 4RC5) within the region (Fig. 2). Further comparison of the sequence alignment (Fig. 2) against the crystal structure of *S. elongatus* PCC 7942 ADO revealed that the remaining substitutions were mainly located on the outer surface of the *Synechococcus* enzyme (Figure SI1).

3.2. Assembly of the heterologous hydrocarbon pathways in E. coli

The genes coding for the selected alternative ADOs were assembled in a pCDF-based *E. coli* expression vector (Table 1), in order to systematically compare the enzymes in a heterologous hydrocarbon production system *in vivo*. The constructs were identical apart from the selected *ado* coding regions, and each gene carried a sequence encoding an N-terminal hexa-Histidine affinity tag to allow isolation (Table 2). The rest of the heterologous hydrocarbon pathway assembled in *E. coli* BL21(DE3)Δ*yqh*DΔ*ahr* was constructed on two additional plasmids with ferredoxin (Fdx), phosphopantetheinyl transferase (ppt) and carboxylic acid reductase (CAR) over-expressed from pET and NADPH: Ferredoxin/Flavodoxin-oxidoreductase (Fpr) from pACYC (Table 1). Altogether, the pathway enabled the *in vivo* conversion of externally supplied C4, C6 and C8 fatty acid precursors into the corresponding C_{n-1} end-

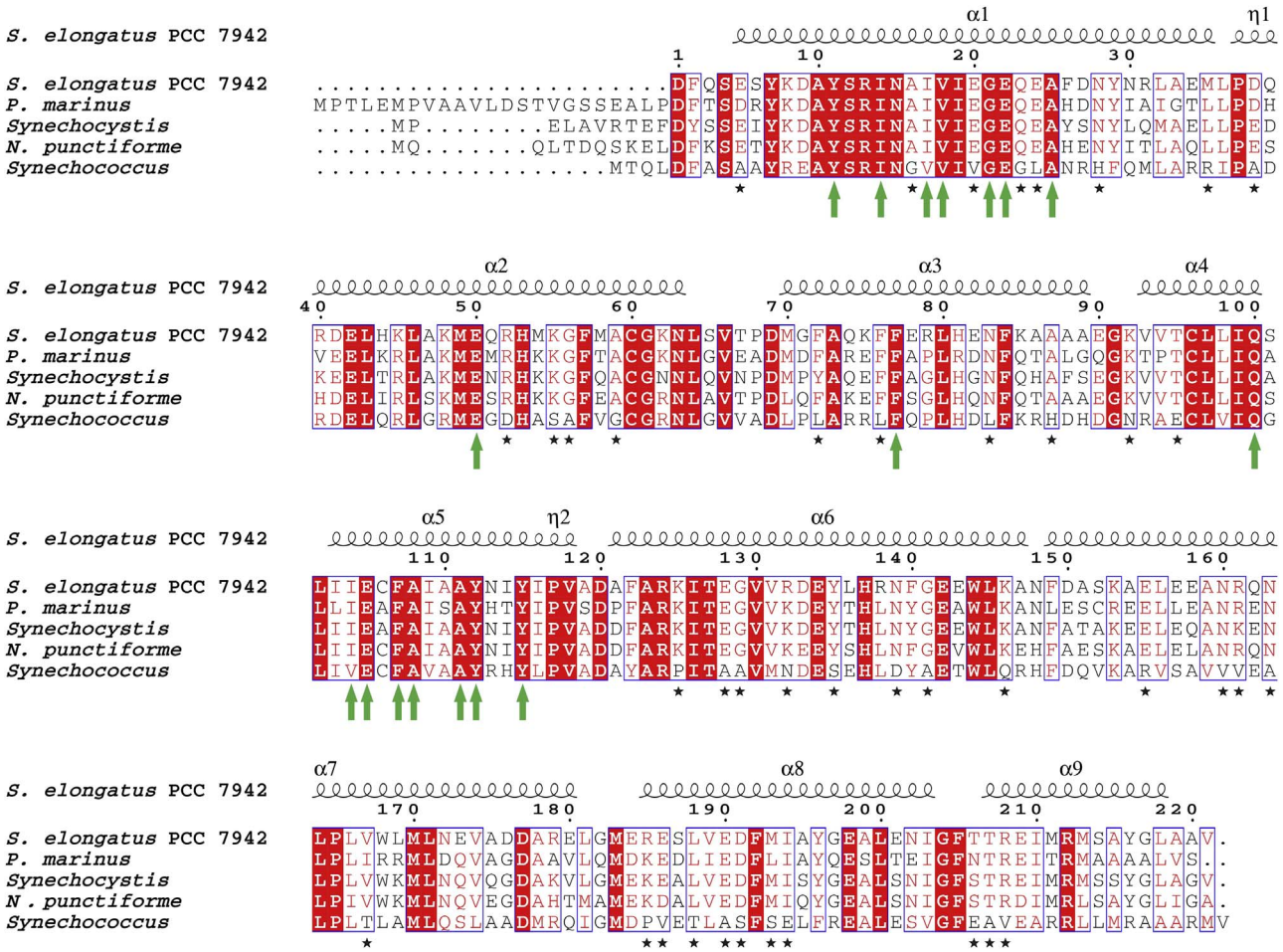

Fig. 2. Amino acid sequence alignment of the five different ADOs compared in the study. The secondary structures and corresponding amino acid numbering shown above the alignment represent the A chain of *S. elongatus* PCC 7942 ADO, as derived from the crystal structure with bound C16 fatty alcohol (PDB code 4RC5) (Jia et al., 2015). The green arrows under the sequence alignment indicate the amino acid residues within 4 Å distance from the fatty alcohol ligand in the 4RC5 complex structure, and the black stars denote the residues which are different in *Synechococcus* ADO in comparison to all the other studied ADO enzymes. (For interpretation of the references to color in this figure legend, the reader is referred to the web version of this article.)

products, propane, pentane and heptane, respectively, followed by quantitation by GC-MS from the headspace of the reaction vials (Kallio et al., 2014).

3.3. Production of heptane from supplied octanoic acid

GC-MS analysis confirmed that all the five parallel *E. coli* strains carrying the heterologous hydrocarbon pathways were able to produce C7 heptane when supplemented with 5 mM octanoic acid in the culture medium. However, there were clear differences in the total production levels as well as the production rates between the systems expressing the different ADO orthologs (Figs. 3A, B, 4). The highest amount of heptane, as measured at the 4 h timepoint, was produced by ADO from *N. punctiforme* (134 $\mu molL^{-1}OD_{600\ nm}{}^{-1}$), while the yield sequentially decreased in the order *P. marinus* A134F (116 $\mu molL^{-1}OD_{600\ nm}{}^{-1}$), *P. marinus* (112 $\mu molL^{-1}OD_{600\ nm}{}^{-1}$) to about 60% of the maximum in *Synechocystis* (81 $\mu molL^{-1}OD_{600\ nm}{}^{-1}$) (Fig. 3A). By far the lowest amount of heptane was produced by ADO from *Synechococcus* (11 $\mu molL^{-1}OD_{600\ nm}{}^{-1}$), which at 4 h was under 10% of the observed maximum (Fig. 3A). The same pattern in the relative ADO activities was obtained in a separate quantitation at the 10 h timepoint (Fig. 3B), although the amount of heptane continued to increase in the case of *P. marinus* and *N. punctiforme* enzymes over the last 6 h.

The rates of heptane production, as depicted from the amount of product accumulated in the vial headspace within the first half an hour of the reaction, also varied between the alternative ADO orthologs (Figs. 3A, 4). The relative rates followed the general pattern of the total productivity, with the ADO from *N. punctiforme* being the most efficient (135 $\mu molL^{-1}OD_{600\ nm}{}^{-1}h^{-1}$), followed by the *P. marinus* variant A134F (77 $\mu molL^{-1}OD_{600\ nm}{}^{-1}h^{-1}$) and the WT enzymes from *P. marinus* (67 $\mu molL^{-1}OD_{600\ nm}{}^{-1}h^{-1}$), *Synechocystis* (55 $\mu molL^{-1}OD_{600\ nm}{}^{-1}h^{-1}$) and *Synechococcus* (2.2 $\mu molL^{-1}OD_{600\ nm}{}^{-1}h^{-1}$).

3.4. Production of pentane from supplied hexanoic acid

All the engineered *E. coli* strains expressing the parallel ADO orthologs produced C5 pentane when supplied with hexanoic acid in the culture medium. Although clear differences were observed in the performance of the alternative ADOs (Figs. 3C, D), the total pentane productivity and the relative differences between the enzymes were smaller than for heptane. While the ADO from *Synechocystis* gave the highest pentane yield (105 $\mu molL^{-1}OD_{600\ nm}{}^{-1}$), the strains expressing the orthologs from *P. marinus* (WT and A134F) and *N. punctiforme* all produced about 80 $\mu molL^{-1}OD_{600\ nm}{}^{-1}$ as measured at the 4 h time-point. The lowest amount of pentane, about 30% of the maximum, was produced by ADO from *Synechococcus* (29 $\mu molL^{-1}OD_{600\ nm}{}^{-1}$). The relative ADO activities determined based on the time-course analysis (Fig. 3C) followed the pattern obtained in a separate quantitation at the 10 h timepoint (Fig. 3D). Again, for the two most efficient enzymes (from *Synechocystis* and *N. punctiforme*), the product accumulation continued over the last 6 h.

The initial rates of pentane production did not in all cases directly

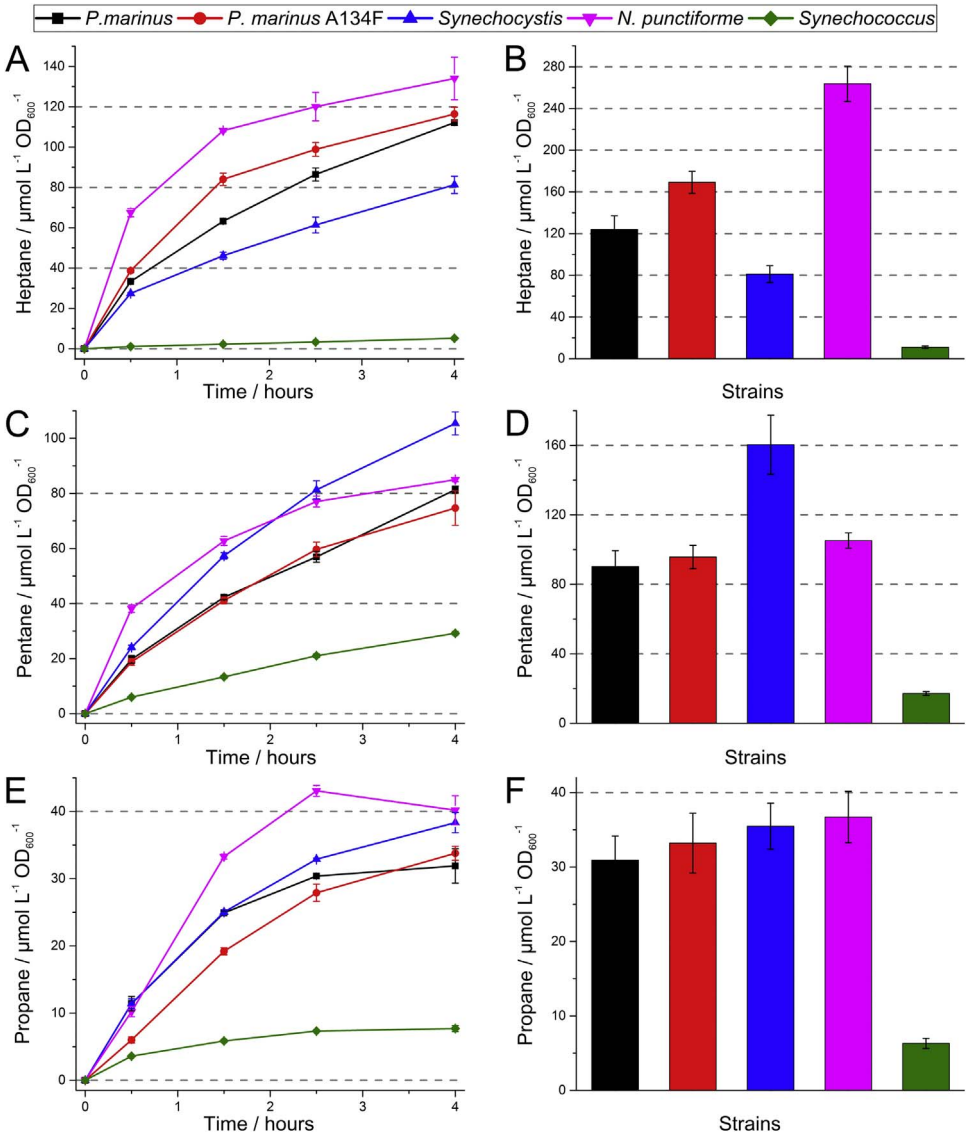

Fig. 3. Alkane production yields of different ADO orthologues expressed in *E. coli*. The time-course analysis between 0 h and 4 h for the production of (A) heptane, (C) pentane and (E) propane, and bars representing the product accumulation at 10 h timepoint for (B) heptane, (D) pentane and (F) propane. The ADOs used in the comparison are from *P. marinus* (black ■), a corresponding variant A134F (red ●), *Synechocystis* (blue ▲), *N. punctiforme* (magenta ▼) and *Synechococcus* (green ♦). Each datapoint represents mean ± SD calculated based on three parallel reactions. (For interpretation of the references to color in this figure legend, the reader is referred to the web version of this article.)

correlate with the final yields; The fastest product accumulation within the first 30 min was measured for the ADO from *N. punctiforme* (77 $\mu molL^{-1}OD_{600\ nm}{}^{-1}h^{-1}$), whereas the ortholog from *Synechocystis* with higher overall production appeared to perform less efficiently (48 $\mu molL^{-1}OD_{600\ nm}{}^{-1}h^{-1}$) (Fig. 4). The initial pentane production rate for the *P. marinus* WT ADO and A134F variant was about equal (~39 $\mu molL^{-1}OD_{600\ nm}{}^{-1}h^{-1}$), and lowest for the ADO from *Synechococcus* (12 $\mu molL^{-1}OD_{600\ nm}{}^{-1}h^{-1}$).

3.5. Production of propane from supplied butanoic acid

When supplied with 5 mM butanoic acid in the culture medium, all the five engineered *E. coli* strains produced propane in the reaction vial headspace (Figs. 3E, F). In comparison to pentane and heptane, the yields of propane were lower (total production below 50% in comparison to the C5 and C7 products), and the differences in the performance of the alternative orthologs less significant (Figs. 3E, F). Apart from the ADO from *Synechococcus* with the lowest propane levels (7.8 $\mu molL^{-1}OD_{600\ nm}{}^{-1}$), the other ADO orthologs produced between 30 and 40 $\mu molL^{-1}OD_{600\ nm}{}^{-1}$ by the 4 h reaction timepoint. Unlike for pentane and heptane, the propane accumulation did not continue after this for any of the strains (Fig. 3E), and the levels remained the same when analyzed at the 10 h timepoint (Fig. 3F).

As for the initial propane production rate, the native ADOs from *N. punctiforme, Synechocystis*, and *P. marinus* performed at near equal efficiency, producing about 20 − 23 $\mu molL^{-1}OD_{600\ nm}{}^{-1}h^{-1}$ (Fig. 4). Interestingly, the initial propane productivity of the *P. marinus* ADO variant A134F (12.0 $\mu molL^{-1}OD_{600\ nm}{}^{-1}h^{-1}$) evaluated based on the first 30 min was only about half of the WT enzyme in the tested *in vivo* system. Again, the ADO from *Synechococcus* had the lowest production efficiency (7.2 $\mu molL^{-1}OD_{600\ nm}{}^{-1}h^{-1}$).

3.6. Expression levels and stability of the ADO enzymes

In order to correlate the hydrocarbon production efficiencies (Figs. 3 and 4) to the relative amounts of the ADO orthologs expressed, the intracellular ADO levels and stability were evaluated for each of the engineered *E. coli* strains. The comparison was carried out by extracting the His-tagged ADO enzymes from the strains at specified timepoints after protein expression, followed by quantitative analysis by Bradford

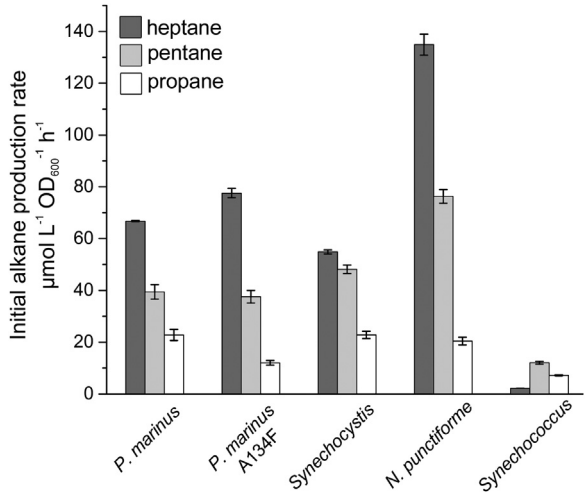

Fig. 4. The initial production rates of heptane (dark grey), pentane (light grey) and propane (white) by the different ADO orthologues. The production rates are depicted from the amount of alkane formed within the first 30 min after sealing the reaction vials. Each column represents mean ± SD calculated from the initial rates of three parallel reactions.

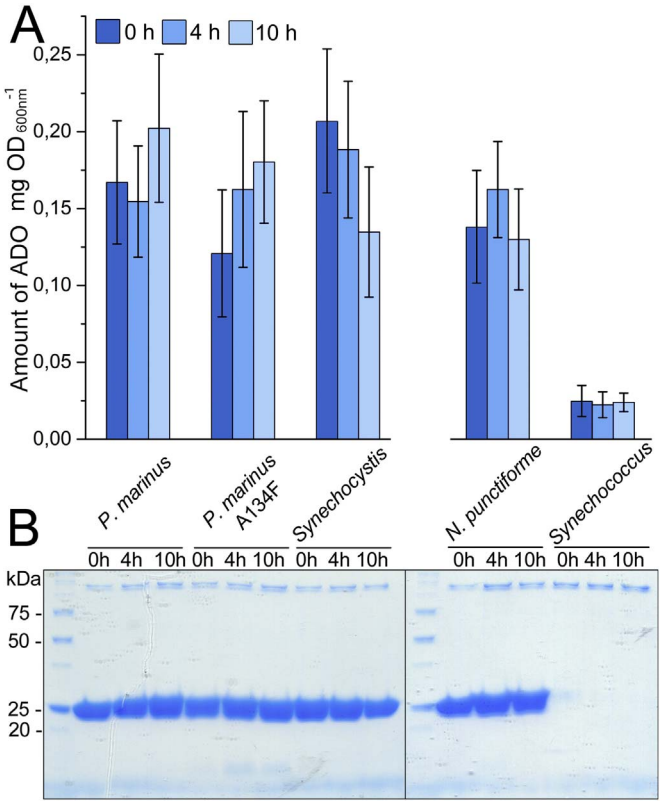

Fig. 5. The expression levels and *in vivo* stability of the ADO enzymes in *E. coli*. (A) The relative amount of His-tag purified ADOs from *E. coli* cells incubated at RT for 0 h (dark blue), 4 h (mid blue) or 10 h (light blue) after the expression phase, quantitated with the Bradford method. (B) SDS-PAGE gel visualizing the ADO purification fractions at different timepoints. Each column represents mean ± SD calculated based on three parallel Bradford reactions. (For interpretation of the references to color in this figure legend, the reader is referred to the web version of this article.)

(Fig. 5A) and SDS-PAGE (Fig. 5B). The first timepoint (0 h) represented the situation at the beginning of the reaction, whereas the subsequent timepoints (4 h and 10 h), after addition of kanamycin to inhibit further protein synthesis in the cells, reflected the overall enzyme stability *in vivo*. The Bradford analysis (Fig. 5A) revealed that the expression levels of four of the ADOs (*Synechocystis*, *N. punctiforme, P. marinus, P. marinus* A134F) were within the same range (0.12–0.20 $mgOD_{600\ nm}{}^{-1}$). In contrast, the amount of the ADO from *Synechococcus* was significantly lower, 11–20% in comparison to the other enzymes. These results were further supported by the SDS-PAGE analysis (Fig. 5B), which confirmed that (i) the purity of the enzyme preparations was high, and that the (ii) ADO levels were rather uniform between the different samples, with the exception of the ADO form *Synechococcus* which was barely visible on the gel. Altogether, the *in vivo* ADO levels remained rather constant throughout the extended incubation at RT, suggesting that enzyme stability in the heterologous host did not have any significant impact on result interpretation.

3.7. ADO mRNA secondary structure analysis in silico

In order to predict and compare mRNA secondary structure formation between the ADO transcripts *in silico*, the homologous sequences were subjected to computational analysis of free energies of potential secondary structures. The prediction performed on the full length ADO mRNAs as well as on the first 170 bases of the transcripts revealed that the lowest free energy of the secondary structures were comparable in all cases (Table SI1), and thus failed to identify divergent structural features which could explain the low expression levels of *Synechococcus* ADO.

3.8. Alcohols produced by endogenous aldehyde reductases

Despite the deletion of two of the endogenous aldehyde reductases in the host genome (Δ*yjgB* Δ*yqhD*), *E. coli* encodes for another 11 homologous enzymes which potentially compete with ADO for the aldehyde substrates (Rodriguez and Atsumi, 2014), and thus may interfere with the hydrocarbon production under evaluation. To study the possible effect of the remaining aldehyde reductases on the outcome, the five generated *E. coli* strains were compared for the production of octanol, hexanol and butanol in response to the supplementation of the three alternative fatty acid substrates. As the primary observation, all the strains were shown to produce alcohols from the respective fatty acids, and despite of specific differences, the overall levels were within the same order of magnitude as measured for the corresponding C_{n-1} alkanes (Fig. 6). Comparison of the parallel biological replicates, as well as independently repeated trials (Figure SI7), showed that the variation between experiments was marginal, suggesting that set-up was applicable for the quantitative analysis of the alcohols. In all cases, only a fraction of the supplemented fatty acid was converted into either of the two products (~7–24%) (Table SI2), indicating that majority of the substrate was always left unreacted with the aldehyde reductases or the ADOs. It was also clear that the fatty acids were not consumed for cell growth, as increase of the OD values was not typically observed during the reaction phase (Table SI3).

As seen in Fig. 6**A-C**, the production of octanol, hexanol and butanol differed clearly from one another in the total levels as well as in the strain-specific patterns. The outcome did not correlate with the substrate chain-length or with the amount of the alkanes produced. Octanol (Fig. 6**A**) was produced at the lowest titers with very subtle differences between the strains, while the hexanol (Fig. 6**B**) and butanol (Fig. 6**C**) profiles showed considerably more variation. This indicated dependence between the production of alkanes and alcohols for the C6/C4 substrates, with maximum alcohol accumulation in the strains expressing the *Synechococcus* ADO.

4. Discussion

4.1. Approach for comparing orthologous ADOs in the production of volatile alkanes

Because of the potential biotechnological applications for generating renewable replacements for petroleum-derived fuels, the cyanobac-

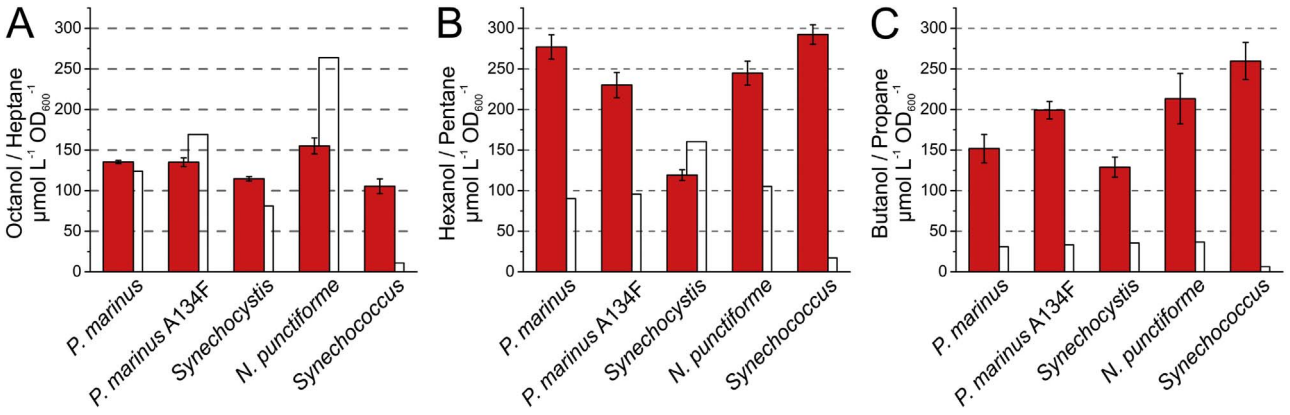

Fig. 6. Alcohol production of the *E. coli* strains under study. The levels of (A) octanol, (B) hexanol and (C) butanol (red bars) were measured with GC-MS after 10 h incubation in response to the supplementation of octanoic acid, hexanoic acid and butanoic acid, respectively. Each bar represents mean ± SD calculated based on three parallel reactions. The corresponding production levels of the respective C_{n-1} alkanes (black outlines; adapted from Fig. 3) are shown to ease direct comparison between the two products. (For interpretation of the references to color in this figure legend, the reader is referred to the web version of this article.)

terial enzyme *aldehyde deformylating oxygenase*, ADO, has been extensively characterized and evaluated as part of various heterologous hydrocarbon production pathways. In this study we conducted a systematic comparison of five alternative ADO orthologs for the production of three short-chain alkanes, heptane, pentane and propane. Short-chain products have been of particular interest because of their volatility under standard atmospheric conditions (Khara et al., 2013; Kallio et al., 2014; Menon et al., 2015; Zhang et al., 2016; Sheppard et al., 2016), which could be exploited for the extraction of the compounds directly from the biotechnological process due to spontaneous separation into the culture head-space. At the same time, while there are general kinetic constraints in the catalytic performance of ADO limiting the development of efficient production systems (Bao et al., 2016; Andre et al., 2013), the capacity of the enzymes to utilize short-chain precursors remains to be especially poor. The ADO orthologs in the current work were selected based on their appearance in literature as representatives of the four major classes of cyanobacteria, as well as the overall limited information on the relative capacity to produce short chain end-products. Despite the numerous studies related to the ADOs from *N. punctiforme* (Schirmer et al., 2010; Warui et al., 2011; Li et al., 2012; Howard et al., 2013; Pandelia et al., 2013; Paul et al., 2013; Hayashi et al., 2015; Rajakovich et al., 2015), *Synechocystis* (Hu et al., 2013; Wang et al., 2013), *Synechococcus* (Schirmer et al., 2010; Harger et al., 2013), *P. marinus* (Schirmer et al., 2010; Krebs et al., 2011; Li et al., 2012; Andre et al., 2013; Khara et al., 2013; Aukema et al., 2013; Buer et al., 2014; Kallio et al., 2014; Zhang et al., 2016) and the *P. marinus* variant A134F (Khara et al., 2013; Menon et al., 2015; Zhang et al., 2016), the enzymes have not been directly compared in a biosynthetic context for the production of volatile hydrocarbons. For this purpose, a novel experimental set-up was constructed based on the earlier analytical system in *E. coli* (Kallio et al., 2014), which enabled the conversion of supplied C8, C6 and C4 fatty acid precursors into the corresponding C_{n-1} alkanes *in vivo* (Fig. 1; Table 1). The strategy was based on the ability of *E. coli* to scavenge fatty acids from the medium into the cell, after which the precursor is reduced into aldehyde by the heterologous enzyme CAR, and further into the final alkane product by ADO. To ensure that the conversion would be primarily limited by ADO, as required for the comparison between the orthologs, additional enzyme components (ppt, Fdx and Fpr) were introduced into the pathway. Ppt is necessary for the optimal function of CAR (Akhtar et al., 2013), while Fdx and Fpr (Kallio et al., 2014), which have not been previously co-expressed in corresponding substrate feeding biotransformation trials, constitute the *in vivo* redox relay for ADO (Fig. 1). For optimizing the performance further, the host strain used for the work was *E. coli* BL21(DE3)Δ*yjgB* Δ*yqhD* (Kallio et al., 2014) from which two genes coding for competing aldehyde reductase enzymes had been deleted. After expression of the pathway enzymes and substrate supplementation, the alkane products were quantitated from the gas-phase of the reaction vials by GC-MS, and statistically compared between the alternative strains.

4.2. Validity of the in vivo strategy for evaluating the performance of alternative ADOs

In order to critically assess the constructed *in vivo* system and to monitor the consistency of the obtained data, all the reactions were carried out in three parallel biological replicates and analyzed in a continuous sequence at successive timepoints. The results showed that (i) the set up enabled the detection of ADO-specific catalytic differences between the orthologs, and that (ii) the variation between replicate samples was marginal in respect to the total signal levels, thus allowing reliable numerical analysis. In addition, the data from the time-course analysis (Figs. 3A, C, E) was further verified in an independent reaction series comparing all the ADOs in parallel in a single experiment (Figs. 3B, D, F), which confirmed that the overall activity pattern was reproducible and that the individual assays could be directly compared between the separate experiments. Altogether, the experimental system appeared to be applicable for comparing the performance of the alternative ADO enzymes in a heterologous biosynthetic context in *E. coli*, and allowed repeatable and statistically-relevant conclusions to be drawn based on the data.

4.3. Differences between ADO expression levels and stability

To evaluate whether the observed differences in the recorded alkane production efficiencies were affected by differences in ADO expression, the amount and stability of the enzymes were studied under the conditions used for the activity assays in the heterologous host. Although there was some variation between the parallel replicates, Bradford assay (Fig. 5A) and SDS-PAGE analysis (Fig. 5B) revealed that there was no significant deviation between the ADOs from *Synechocystis*, *N. punctiforme, P. marinus* or *P. marinus* A134F which would affect the comparison. The only ortholog present in clearly lower amount was ADO from *Synechococcus*, which also shared the lowest sequence conservation amongst the enzymes. As the promoter and the ribosome binding site (RBS) region of all the constructs were identical, and the computational free energy prediction of mRNA secondary structures failed to identify obvious differences between the transcripts (Table SI1), the low abundance could reflect constraints at the enzyme-level. Majority of the conserved amino acid substitutions found specifically in the *Synechococcus* ADO are located on the outer surface of the enzyme (Fig. 2, SI1), and these could potentially contribute to unoptimal

folding causing premature degradation. Such conformational defects could also affect the integrity of the binding site pocket and interfere with the substrate-enzyme interactions, which would explain the observed reduced capacity of the *Synechococcus* ADO to utilize the C8 substrate (Fig. 3A).

4.4. Production of alcohols by the endogenous aldehyde reductases

The production of alkanes was shown to be accompanied by the accumulation of the corresponding alcohols, as expected based on the wide range of endogenous aldehyde reductases still present in the *E. coli* host. Generally the recorded alcohol levels were somewhat higher in comparison to the alkanes, but remained within a similar overall molar range (Fig. 6). At the same time, majority of the supplemented fatty acid substrates were not converted into either of the products (Table SI2) nor used for cell growth (Table SI3), implying that access to the substrates would not be the primary limiting factor in the systems. While the two alternative pathways appeared to have a rather insignificant effect on another in the case of the C8 precursor, as suggested by the constant octanol production levels of the parallel strains (Fig. 6A), the observed variation in the hexanol (Fig. 6B) and butanol (Fig. 6C) profiles indicate competition between the aldehyde reductases and ADO. Considering the relative output levels and the amount of available substrates, however, the concomitant formation of alcohols was not expected to alter the overall alkane production patterns to a degree which would significantly alter data interpretation or the conclusions of the study.

4.5. Substrate-specific characteristics common to all the pathways

All five ADO orthologs were shown to be active, and produced heptane, pentane and propane in the headspace of the reaction vials from the supplied C8, C6 and C4 fatty acid substrates, respectively. There were certain general substrate-specific patterns, however, which were common to the ADO enzymes. As a clear trend, the overall productivities decreased in correlation with the substrate chain length (Fig. 3). At the same time, the initial reaction rates were slower for the shorter substrates (Fig. 4), and the plateau was reached much earlier for butanoic acid in comparison to the longer fatty acids (Fig. 3). These observations are in agreement with the reported kinetic constraints of the ADO enzymes towards shorter precursors (Khara et al., 2013) (Kallio et al., 2014) (Bao et al., 2016), and reflect lower affinity (K_M) and overall catalytic efficiency (apparent k_{cat}/K_M) towards substrates outside the native chain-length range. While the comparison demonstrates that ADO substrate-specific properties can be quantitatively evaluated in defined biosynthetic contexts *in vivo* for volatile products, it must be noted that the overall kinetics are also affected by rate of substrate diffusion into the cell, the efficiency of the previous enzymatic step by CAR (Fig. 1) and the affinity of the remaining endogenous aldehyde dehydrogenases for the precursors, which all need to be accounted for.

4.6. ADO-specific characteristics in volatile hydrocarbon production

The comparative analysis revealed clear enzyme-specific differences between the alternative ADOs both in the total productivity (Fig. 3) and the initial reaction rates (Fig. 4) for all of the evaluated substrates. Judged based on the combined data, the ADO from *N. punctiforme* appeared to perform better than the other orthologs. The production yields of heptane, for example, were several folds higher in comparison to the enzymes from *P. marinus* or *Synechocystis* (Fig. 3B). Also the initial production rates of the *N. punctiforme* enzyme were highest in most cases, especially for heptane and pentane (Fig. 4). This is in line with the reported superior activity of the *N. punctiforme* ADO in respect to the native products pentadecane and heptadecene (Schirmer et al., 2010), suggesting that the observed effect is not chain-length specific but related to other catalytic properties than mere substrate preference. Interestingly, the *P. marinus* ADO variant A134F which has previously been shown to have higher preference for shorter precursors (Khara et al., 2013; Sheppard et al., 2016) performed slightly better for the C8 substrate, while the activity towards C6 and C4 aldehydes remained at the WT levels. This may be due to variations in the local substrate concentrations between alternative experimental set-ups, which could result in differences in the observed K_M -dependent catalytic efficiencies. By far the lowest activities were recorded for the system harboring ADO from *Synechococcus* (Figs. 3 and 4). Taking into account the very low levels of the enzyme in the cells (Fig. 5), however, the specific activity and the overall kinetic parameters may not differ so much from those of the other orthologs. The inferior performance of the *Synechococcus* ADO has been observed already earlier (Schirmer et al., 2010), which confirms that this is not specific to the current experimental set-up, but rather an intrinsic property of the enzyme. The only clear deviations in the catalytic patterns of the ADOs were the unexpectedly high activity of *Synechocystis* enzyme for pentane (Figs. 3C, D), and the low activity of the *Synechococcus* enzyme for heptane (Figs. 3A, B). These trends were repeatable and apparent in the separate independent reactions series, and expected to reflect enzyme-specific traits on substrate preference, which cannot be predicted based on the currently existing structural and functional data.

5. Conclusions

In this study, five different cyanobacterial ADO enzymes were evaluated *in vivo* in a novel biosynthetic context in *E. coli* for the production of short-chain volatile alkanes, heptane, pentane and propane. The comparison, based on supplemented fatty acid precursors, provided new insight into the catalytic performance of the ADOs, with information on the relative production efficiencies and substrate specificities between the enzymes. The study revealed common substrate-specific characteristics of the ADOs, as well as clear enzyme-specific differences in the catalytic performance. The observed variation in the production of the volatile alkanes between the ADOs is not obvious at amino acid level, but the information may still provide new perspectives into the detailed structural comparison in respect to kinetic traits of the different orthologs. The results also demonstrated that endogenous aldehyde reductases of the *E. coli* host exhibit affinity towards the C4-C8 aldehyde substrates, which must be taken into consideration when evaluating ADO-based microbial production systems for short-chain volatile alkanes.

Acknowledgements

This work was supported by TEKES (#40128/2014) and the Academy of Finland (#271832, #272424). The Authors acknowledge Neil Marsh (University of Michigan, USA) and Nigel Scrutton (The University of Manchester, UK) for providing the original expression constructs for the *P. marinus* ADO. The Authors thank Vesa Havurinne for the help at the initial phase of construct assembly.

Appendix A. Supporting information

Supplementary data associated with this article can be found in the online version at http://dx.doi.org/10.1016/j.meteno.2017.05.001.

References

Akhtar, M.K., Turner, N.J., Jones, P.R., 2013. Carboxylic acid reductase is a versatile enzyme for the conversion of fatty acids into fuels and chemical commodities. Proc. Natl. Acad. Sci. USA 110, 87–92.

Altschul, S.F., Gish, W., Miller, W., Myers, E.W., Lipman, D.J., 1990. Basic local alignment search tool. J. Mol. Biol. 215, 403–410.

Andre, C., Kim, S.W., Yu, X.H., Shanklin, J., 2013. Fusing catalase to an alkane-producing enzyme maintains enzymatic activity by converting the inhibitory byproduct H2O2

to the cosubstrate O2. Proc. Natl. Acad. Sci. USA 110, 3191–3196.
Aukema, K.G., Makris, T.M., Stoian, S.A., Richman, J.E., Münck, E., Lipscomb, J.D., Wackett, L.P., 2013. Cyanobacterial Aldehyde Deformylase Oxygenation of Aldehydes Yields n – 1 Aldehydes and Alcohols in Addition to Alkanes. ACS Catal. pp. 2228–2238.
Bao, L., Li, J.J., Jia, C., Li, M., Lu, X., 2016. Structure-oriented substrate specificity engineering of aldehyde-deformylating oxygenase towards aldehydes carbon chain length. Biotechnol. Biofuels 9, 185.
Bradford, M.M., 1976. A rapid and sensitive method for the quantitation of microgram quantities of protein utilizing the principle of protein-dye binding. Anal. Biochem. 72, 248–254.
Buer, B.C., Paul, B., Das, D., Stuckey, J.A., Marsh, E.N., 2014. Insights into substrate and metal binding from the crystal structure of cyanobacterial aldehyde deformylating oxygenase with substrate bound. ACS Chem. Biol. 9, 2584–2593.
Choi, Y.J., Lee, S.Y., 2013. Microbial production of short-chain alkanes. Nature 502, 571–574.
Coates, R.C., Podell, S., Korobeynikov, A., Lapidus, A., Pevzner, P., Sherman, D.H., Allen, E.E., Gerwick, L., Gerwick, W.H., 2014. Characterization of cyanobacterial hydrocarbon composition and distribution of biosynthetic pathways. PLoS One 9, e85140.
Das, D., Eser, B.E., Han, J., Sciore, A., Marsh, E.N., 2011. Oxygen-independent decarbonylation of aldehydes by cyanobacterial aldehyde decarbonylase: a new reaction of diiron enzymes. Angew. Chem. Int. Ed. Engl. 50, 7148–7152.
Harger, M., Zheng, L., Moon, A., Ager, C., An, J.H., Choe, C., Lai, Y.L., Mo, B., Zong, D., Smith, M.D., Egbert, R.G., Mills, J.H., Baker, D., Pultz, I.S., Siegel, J.B., 2013. Expanding the product profile of a microbial alkane biosynthetic pathway. ACS Synth. Biol. 2, 59–62.
Hayashi, Y., Yasugi, F., Arai, M., 2015. Role of cysteine residues in the structure, stability, and alkane producing activity of cyanobacterial aldehyde deformylating oxygenase. PLoS One 10, e0122217.
Howard, T.P., Middelhaufe, S., Moore, K., Edner, C., Kolak, D.M., Taylor, G.N., Parker, D.A., Lee, R., Smirnoff, N., Aves, S.J., Love, J., 2013. Synthesis of customized petroleum-replica fuel molecules by targeted modification of free fatty acid pools in Escherichia coli. Proc. Natl. Acad. Sci. USA 110, 7636–7641.
Hu, P., Borglin, S., Kamennaya, N.A., Chen, L., Park, H., Mahoney, L., Kijac, A., Shan, G., Chavarría, K.L., Zhang, C., Quinn, N.W.T., Wemmer, D., Holman, H.-Y., Jansson, C., 2013. Metabolic phenotyping of the cyanobacterium Synechocystis 6803 engineered for production of alkanes and free fatty acids. Appl. Energy 102, 850–859.
Jia, C., Li, M., Li, J., Zhang, J., Zhang, H., Cao, P., Pan, X., Lu, X., Chang, W., 2015. Structural insights into the catalytic mechanism of aldehyde-deformylating oxygenases. Protein Cell 6, 55–67.
Kaiser, B.K., Carleton, M., Hickman, J.W., Miller, C., Lawson, D., Budde, M., Warrener, P., Paredes, A., Mullapudi, S., Navarro, P., Cross, F., Roberts, J.M., 2013. Fatty aldehydes in cyanobacteria are a metabolically flexible precursor for a diversity of biofuel products. PLoS One 8, e58307.
Kallio, P., Pásztor, A., Thiel, K., Akhtar, M.K., Jones, P.R., 2014. An engineered pathway for the biosynthesis of renewable propane. Nat. Commun. 5, 4731.
Khara, B., Menon, N., Levy, C., Mansell, D., Das, D., Marsh, E.N., Leys, D., Scrutton, N.S., 2013. Production of Propane and Other Short-Chain Alkanes by Structure-Based Engineering of Ligand Specificity in Aldehyde-Deformylating Oxygenase. Chembiochem 14, 1204–1208.
Krebs, C., Bollinger, J.M., Booker, S.J., 2011. Cyanobacterial alkane biosynthesis further expands the catalytic repertoire of the ferritin-like 'di-iron-carboxylate' proteins. Curr. Opin. Chem. Biol. 15. pp. 291–303.
Li, N., Chang, W.C., Warui, D.M., Booker, S.J., Krebs, C., Bollinger, J.M., 2012. Evidence for only oxygenative cleavage of aldehydes to alk(a/e)nes and formate by cyanobacterial aldehyde decarbonylases. Biochemistry 51. pp. 7908–7916.
Marsh, E.N., Waugh, M.W., 2013. Aldehyde Decarbonylases: enigmatic Enzymes of Hydrocarbon Biosynthesis. ACS Catal. 3 (11), 2515–2521.
Menon, N., Pásztor, A., Menon, B.R., Kallio, P., Fisher, K., Akhtar, M.K., Leys, D., Jones, P.R., Scrutton, N.S., 2015. A microbial platform for renewable propane synthesis based on a fermentative butanol pathway. Biotechnol. Biofuels 8, 61.
Pandelia, M.E., Li, N., Nørgaard, H., Warui, D.M., Rajakovich, L.J., Chang, W.C., Booker, S.J., Krebs, C., Bollinger, J.M., 2013. Substrate-triggered addition of dioxygen to the diferrous cofactor of aldehyde-deformylating oxygenase to form a diferric-peroxide intermediate. J. Am. Chem. Soc. 135. pp. 15801–15812.
Paul, B., Das, D., Ellington, B., Marsh, E.N., 2013. Probing the mechanism of cyanobacterial aldehyde decarbonylase using a cyclopropyl aldehyde. J. Am. Chem. Soc. 135, 5234–5237.
Rajakovich, L.J., Nørgaard, H., Warui, D.M., Chang, W.C., Li, N., Booker, S.J., Krebs, C., Bollinger, J.M., Pandelia, M.E., 2015. Rapid Reduction of the Diferric-Peroxyhemiacetal Intermediate in Aldehyde-Deformylating Oxygenase by a Cyanobacterial Ferredoxin: evidence for a Free-Radical Mechanism. J. Am. Chem. Soc. 137. pp. 11695–11709.
Reuter, J.S., Mathews, D.H., 2010. RNAstructure: software for RNA secondary structure prediction and analysis. BMC Bioinform. 11, 129.
Robert, X., Gouet, P., 2014. Deciphering key features in protein structures with the new ENDscript server. Nucl. Acids Res. 42, W320–4.
Rodriguez, G.M., Atsumi, S., 2014. Toward aldehyde and alkane production by removing aldehyde reductase activity in Escherichia coli. Metab. Eng. 25, 227–237.
Schirmer, A., Rude, M., Li, X., Popova, E., del Cardayre, S., 2010. Microbial biosynthesis of alkanes. Science 329, 559–562.
Sheppard, M.J., Kunjapur, A.M., Prather, K.L., 2016. Modular and selective biosynthesis of gasoline-range alkanes. Metab. Eng. 33, 28–40.
Song, X., Yu, H., Zhu, K., 2016. Improving alkane synthesis in Escherichia coli via metabolic engineering. Appl. Microbiol. Biotechnol. 100, 757–767.
Tan, X., Yao, L., Gao, Q., Wang, W., Qi, F., Lu, X., 2011. Photosynthesis driven conversion of carbon dioxide to fatty alcohols and hydrocarbons in cyanobacteria. Metab. Eng. 13, 169–176.
Wang, Q., Huang, X., Zhang, J., Lu, X., Li, S., Li, J.J., 2014. Engineering self-sufficient aldehyde deformylating oxygenases fused to alternative electron transfer systems for efficient conversion of aldehydes into alkanes. Chem. Commun. 50, 4299–4301.
Wang, W., Liu, X., Lu, X., 2013. Engineering cyanobacteria to improve photosynthetic production of alka(e)nes. Biotechnol. Biofuels 6, 69.
Warui, D.M., Li, N., Nørgaard, H., Krebs, C., Bollinger, J.M., Booker, S.J., 2011. Detection of formate, rather than carbon monoxide, as the stoichiometric coproduct in conversion of fatty aldehydes to alkanes by a cyanobacterial aldehyde decarbonylase. J. Am. Chem. Soc. 133. pp. 3316–3319.
Zhang, L., Liang, Y., Wu, W., Tan, X., Lu, X., 2016. Microbial synthesis of propane by engineering valine pathway and aldehyde-deformylating oxygenase. Biotechnol. Biofuels 9, 80.